Concert Exploration of DFIG Grid-integrated MMC using Artificial Intelligence

Navya Kuchkulla
Department of Electrical Engineering, Osmania University, India
knavya9999@gmail.com (Corresponding author)

Mallesham Gaddam
Department of Electrical Engineering, Osmania University, India
drgm@osmania.ac.in

Narasimhulu V
Department of Electrical & Electronics Engineering, Rajeev Gandhi Memorial College of Engineering and Technology (Autonomous), India
heee.sdit@gmail.com

Received: 8 June 2023 | Revised: 25 June 2023 | Accepted: 29 June 2023

Licensed under a CC-BY 4.0 license | Copyright (c) by the authors | *DOI: https://doi.org/10.48084/etasr.6109*

ABSTRACT

The performance of grid-connected wind turbine systems that use a Doubly Fed Induction Generator (DFIG) is explored in this work. In the suggested configuration, two conversion stages are present. In the first step, Alternating Current (AC) voltage is changed into Direct Current (DC) voltage. At this point, the conventional two-level converter is implemented. The second stage involves the conversion of DC to AC using a five-level Modular Multilevel Converter (MMC). Voltage fluctuation is observed in the DC link. It is anticipated that the Fuzzy Logic Control (FLC) approach will be able to adjust the DC link voltage at the MMC of the second stage of conversion. For the purpose of the Pulse Width Modulation (PWM) system, the current controller is accountable for regulating the current signals and the reference signals. As a result, the PI Controller (PIC) is being evaluated for use in this function. Carrier-based Phase Disposition (PD) PWM is employed for MMC switch control. The proposed controllers' performance is validated in Matlab/Simulink.

Keywords-DC link Voltage; DFIG; FLC; Modular Multilevel Converter (MMC); PI; Pulse Width Modulation (PWM); WECS; RSC

I. INTRODUCTION

Globally, governments are forced to search for alternative renewable energy sources due to worries over pollution and energy constraints. A wide variety of wind power systems have been established during the last two decades, enhancing conversion efficiency and lowering the cost of wind power generation. Various types of DFIGs [1-8] have been published, and many of them are being employed in practice. Wound rotor generators with slip rings are conventional DFIGs. A standard type switch is used in all topologies. Power electronic switches [9] of several sorts can be utilized, however the Insulated Gate Bipolar Transistor (IGBT) is the utmost often used, along with 2-level topologies and AC-voltages below 1kV. The voltage control of the DC link [10-12] is the key issue in grid connected voltage source converters [13]. The PI and FLCs [14-19] are the methods used for balancing the DC voltage. In this paper, FLC is projected to regulate the DC voltage in a DFIG integrated to the grid. Generally standard two level converters [20-21] are adopted in grid interfacing DFIG applications. The multilevel inverter [22-24] is very attractive in various applications due to the production of fewer harmonics and a modular structure comparable to traditional converters' [25-26]. MMCs [27-28] are receiving popularity recently due to their modularity in structure and less harmonic content in the output voltage and current. The Half Bridge (HB) type of the sub module is adopted. The carrier based Phase Disposition (PD) PWM is adopted for the control of IGBTs. The DFIG [30-31] wind turbine based grid connected system is considered in this paper. The rectifier and inverter are required for the integration of a three phase grid. Hence, the HB sub module based MMC 5-level inverter is studied in this article. The DC voltage balance problem is investigated in the MMC grid connected system. Hence, the artificial intelligence based FLC is projected in this article and the comparative results using PI and FLC are presented.

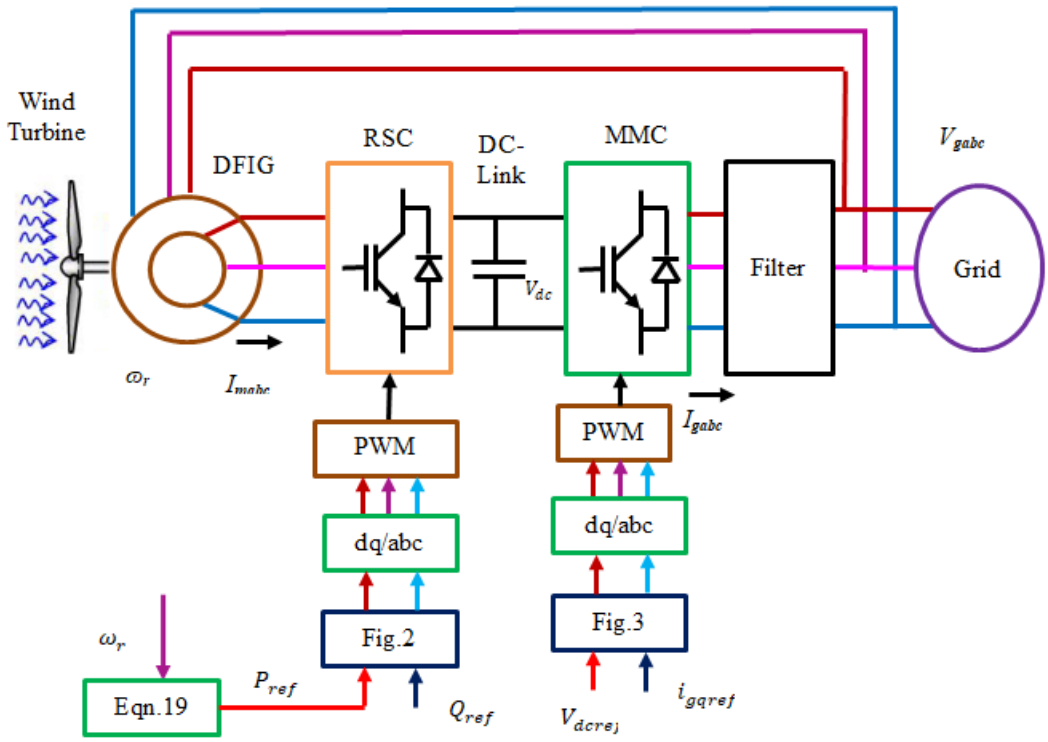

Fig. 1. Block diagram of DFIG WECS.

II. METHODOLOGY

Wind energy can be converted into mechanical energy through the usage of wind turbines. Based on aerodynamic principles, the wind turbine output power is stated as follows:

$$P_t = \frac{1}{2}\rho\pi R^2 v_v^3 C_p \quad (1)$$

$$T_t = \frac{1}{2}\rho\pi R^3 v_v^2 C_p \quad (2)$$

When simulating a DFIG, the flux linkage is the basic variable that is chosen to represent the *d-q* axis. The Park model serves as the foundation for this representation, which is built on two axes full-order. There is a representation of three axes that is analogous to it, but only uses two axes. In this case, the direct axis of the stator is denoted by *ds* and the quadrature axis by *qs*. The direct axis of the rotor is denoted by *dr*, and the quadrature axis of the rotor is denoted by *qr*. Here, the synchronously rotating *d-q* reference frame is being utilized. Within the confines of this framework, three-phase quantities are converted into their corresponding two-phase equivalents. The voltage equations are presented in (3)-(6) and the flux linkages are listed in (7)-(10). Electromagnetic torque is presented in (11):

$$V_{ds} = R_s i_{ds} + \frac{d\varphi_{ds}}{dt} - j\omega_s\varphi_{qs} \quad (3)$$

$$V_{qs} = R_s i_{qs} + \frac{d\varphi_{qs}}{dt} + j\omega_s\varphi_{ds} \quad (4)$$

$$V_{dr} = R_r i_{dr} + \frac{d\varphi_{dr}}{dt} + j(\omega_s - \omega_m)\varphi_{qr} \quad (5)$$

$$V_{qr} = R_r i_{qr} + \frac{d\varphi_{qr}}{dt} - j(\omega_s - \omega_m)\varphi_{dr} \quad (6)$$

$$\varphi_{ds} = L_s I_{ds} + L_m I_{dr} \quad (7)$$

$$\varphi_{qs} = L_s I_{qs} + L_m I_{qr} \quad (8)$$

$$\varphi_{dr} = L_r I_{dr} + L_m I_{ds} \quad (9)$$

$$\varphi_{qr} = L_r I_{qr} + L_m I_{qs} \quad (10)$$

$$T_{em} = \frac{3}{2} p \frac{L_m}{L_s} \left(\varphi_{qs} i_{dr} - \varphi_{ds} i_{qr}\right) \quad (11)$$

For the mechanical part:

$$\frac{d\omega_r}{dt} = \frac{p}{J}(T_e - T_m) \quad (12)$$

$$\frac{d\theta_r}{dt} = \omega_r \quad (13)$$

The power equations are presented in (14)-(17):

$$P_s = \frac{3}{2}\left(V_{ds} i_{ds} + V_{qs} i_{qs}\right) \quad (14)$$

$$P_r = \frac{3}{2}\left(V_{dr} i_{dr} + V_{qr} i_{qr}\right) \quad (15)$$

$$Q_s = \frac{3}{2}\left(V_{ds} i_{ds} + V_{qs} i_{qs}\right) \quad (16)$$

$$Q_r = \frac{3}{2}\left(V_{dr} i_{dr} + V_{qr} i_{qr}\right) \quad (17)$$

P_{ref} is obtained using (18) and (19), where λ refers to the tip speed ratio, R to the length of blades, and v to the wind velocity.

$$\lambda = \frac{R\omega_r}{v} \quad (18)$$

$$P_{ref} = k_{opt}\lambda \quad (19)$$

Because there is no circulation channel in a 3-phase system, it is not required to consider zero sequence components in the system. Equation (20) depicts the three-phase balanced voltages:

$$\begin{bmatrix} V_{ga} \\ V_{gb} \\ V_{gc} \end{bmatrix} = V_m \begin{bmatrix} \sin \omega t \\ \sin(\omega t + 120^0) \\ \sin(\omega t - 120^0) \end{bmatrix} \quad (20)$$

The DFIG connection is depicted in Figure 1. Control structure of RSC [10] is illustrated in Figure 2. Actual power (P_{actual}) is fed from the DFIG and compared with the reference value. Equation (19) determines the power reference value. The control for the RSC is made up of two control loops, which together make up the secondary voltage control loop.

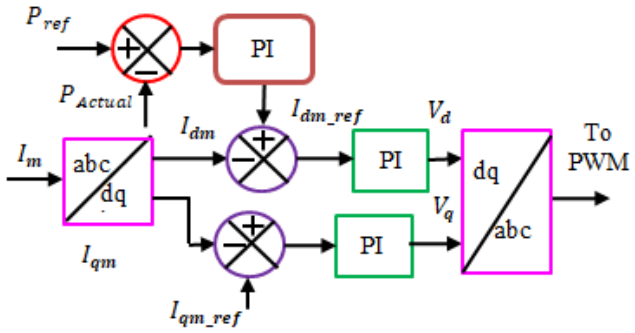

Fig. 2. Control block diagram of RSC.

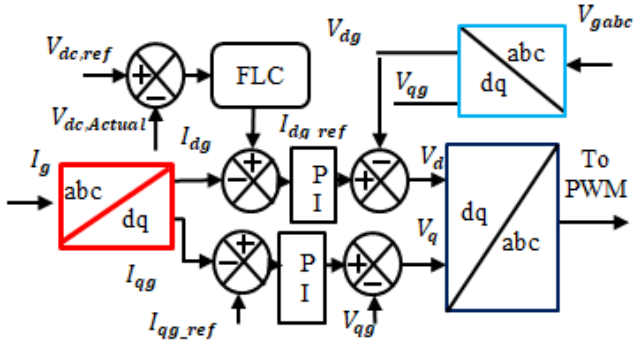

Fig. 3. Control illustration of GSC.

The primary responsibility of the GSC is to continue a voltage that is continuous across the DC link. Figure 3 presents the controller block illustration that describes the control mechanism of the GSC. The current allusion signal (I_{dg_ref}) is produced by adopting the FLC method. FLC is responsible for producing the allusion *d*-axis grid current. The *d*-*q* axis grid voltage is produced by the inner current controller, which does this by mixing the *d*-axis allusion grid current with the actual *d*-axis grid current. After that, the voltage components of the 3-phase *abc* grid are transferred to the gate firing generator, which is responsible for generating the MMC firing pulses. The HB based sub module is used as depicted in Figure 4. The Sub-Modules (SMs) are connected in series to produce the multilevel output voltage in a step-by-step fashion. By linking an *N* number of SM in series, the *N*+1 level can be achieved. Each SM has a capacitor, and the voltage is divided by the number of sub-modules *N*. If switch S_1 is turned ON and the S_2 is turned OFF, then the SM voltages is V_0, and reverse operation results in a SM voltage of zero. Table I shows the various stages of SM along with the relevant output voltage.

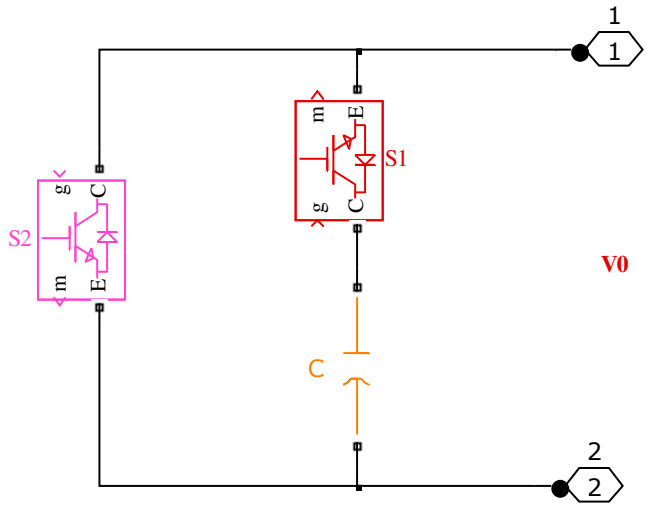

Fig. 4. HB sub module.

TABLE I. SUB-MODULE SWITCHING STATES AND ITS OUTPUT VOLTAGE [20]

Mode	S_1	S_2	Output Voltage
1	IGBT ON	IGBT OFF	V_0
2	IGBT OFF	IGBT ON	0

The equation for the PI controller output $u(t)$ in the time domain is:

$$u(t) = K_p e(t) + K_i \int e(t)\mathrm{d}t \quad (21)$$

A triangular type Membership Function (MF) is considered in this work. The FIS system of the FLC comprises two input functions and 49-rules are obtained. The 7×7 rules based MFs are noted in Table II. The Mamdani type of FIS system is adopted in this work:

$$NFR = NMF^{NI} \quad (22)$$

The quantity of the MFs is denoted by *NMF*, the quantity of inputs by *NI*, and the number of fuzzy rules by *NFR*.

TABLE II. MF RULES

		Error						
		NL	NM	NS	Z	PS	PM	PL
Change of error	NL	NL	NL	NL	NL	NM	NS	Z
	NM	NL	NL	NL	NM	NS	Z	PS
	NS	NL	NL	NM	NS	Z	PS	PM
	Z	NL	NM	NS	Z	PS	PM	PL
	PS	NM	NS	Z	PS	PM	PL	PL
	PM	NS	Z	PS	PM	PL	PL	PL
	PL	NL	NM	NS	Z	PS	PM	PL

P L = Positive Large, N L=Negative Large, P M=Positive Moderate, N M=Negative Moderate, N S=Negative Small, P S=Positive Small, and Z=Zero.

The proposed configuration is simulated using PI and FLC. The comparative performance parameters including reactive power, active power, THD, and DC link voltage balance are addressed in this paper. Table III contains the simulation parameters. A grid voltage of 400 V is considered. The DC ink reference voltage is set at 650 V by (23):

$$V_{dc\ ref} = \frac{2\sqrt{2} \times Vgridrms}{\sqrt{3} \times m} \quad (23)$$

*w*here m is the modulation index.

The simulation is done for the proposed system in two cases. In case 1, the PI controller is adopted and its response waveforms are presented in Figure 5. In case 2, the FLC is implemented and its results are illustrated in Figure 6. Grid Voltage of 400 V and current of 73.05 A are obtained and their waveforms are illustrated in Figure 5(a)-(b). The apparent power, active power, reactive power values are 49632 VA, 42,879 W and -24,994 Var. Figure 5(f) provides an illustration of the voltage across the dc link. Figure 5(g) depicts the grid current Total Harmonic Distortion (THD). The grid current THD using PI controller is 4.79%. When using the FLC controller a grid voltage of 400 V and a current of 75 A are obtained and their waveforms are shown in Figure 6(a)-(b). The apparent power, active power, reactive power values are 49968 VA, 44185 W and -23335 Var. Figure 6(f) provides an illustration of the voltage across the DC link. Figure 6(g) depicts the grid current THD, which is 4.14% and outperforms the PI controller.

The DC voltage comparison of the proposed MMC in DFIG configuration using PI and FLC is depicted in Figure7. It can be observed that the DC voltage does not have a balanced relationship with the PI controller. The FLC controller has ensured that the DC voltage is balanced, and it is tracking the reference value of 650V. This improvement leads the effectiveness of the controller performance.

TABLE III. SPECIFICATIONS

Description	Value
Resistance, inductance (stator)	0.01965 p. u, 0.0397 p.u
Voltage	400 V
Resistance (rotor)	0.01909 p.u
Mutual inductance	1.354 p.u
Speed	1.2 p.u
Friction factor, No. of pole-pairs	0.05479 p.u, 2
Inertia constant	0.09526
Capacitor	4700 µF
DC voltage	650 V
Filter inductance	5.35 mH
Grid Voltage, grid frequency	400 V, 50 Hz
Grid resistance and inductance	0.01 Ω, 0.02 mH
Wind velocity	12 m/s

TABLE IV. SIMULATION RESULTS

Parameter	PI controller	FLC
Apparent power (VA)	49,632	49,968
Active power (W)	42,879	44,185
Reactive power (VAR)	-24,994	-23,335
DC Voltage (V)	600	650
DC Voltage settling time (s)	Not settled	0.4
Grid current THD (%)	4.79	4.14

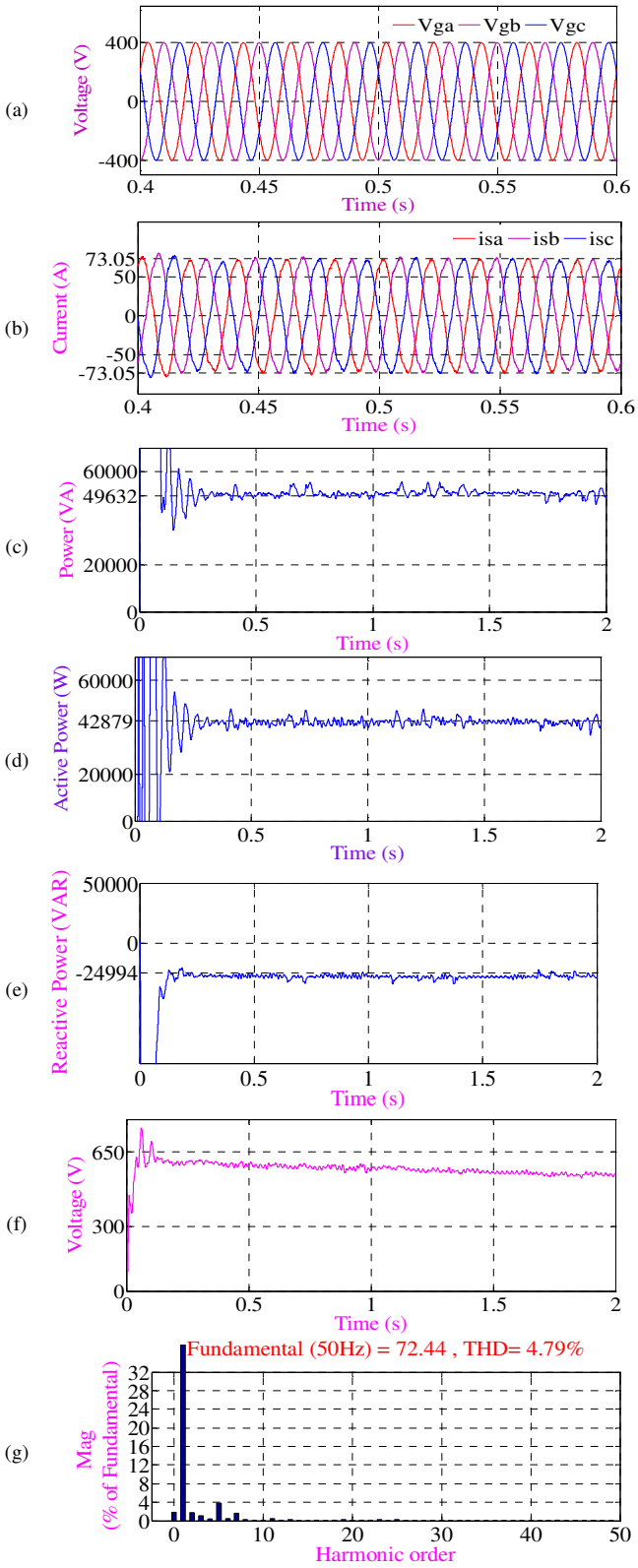

Fig. 5. Response waveforms with the PI controller: (a) Grid Voltage, (b) grid current, (c) apparent power, (d) active power, (e) reactive power, (f) DC link Voltage, (g) THD.

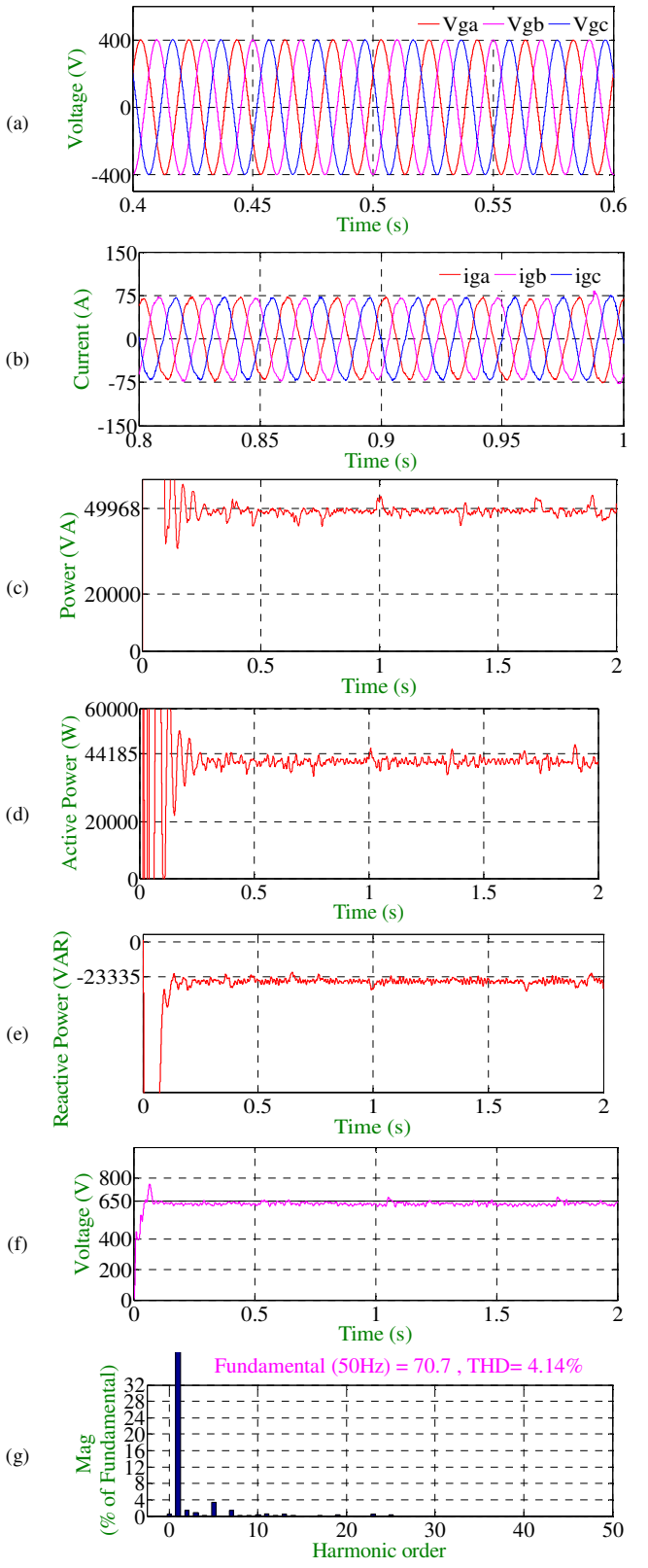

Fig. 6. Response waveforms with the FLC controller: (a) Grid Voltage, (b) grid current, (c) apparent power, (d) active power, (e) reactive power, (f) DC link Voltage, (g) THD.

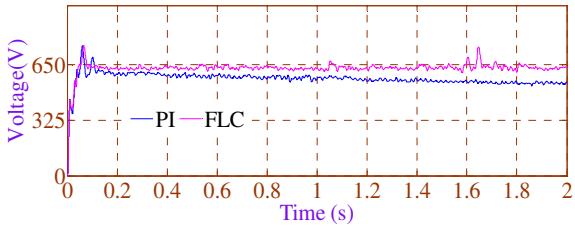

Fig. 7. DC voltage comparison.

III. CONCLUSION

The mathematical modeling of the DFIG and the grid is described in detail in this paper. There are two converters involved in the modeling of the grid-connected DFIG. The converters used at the rotor side the grid side are called RSC and GSC, respectively. The RSC is effectively controlled by a PI controller. The standard two-level converter is systematically controlled. The 5-level MMC with HB SB is modeled and controlled effectively with advanced PD PWM. The proposed control scheme's effectiveness was evaluated. It is clear from the data that the machine side parameters can monitor their reference. The proposed controller achieves optimum DC voltage regulation. The effectiveness of the proposed controller is evaluated by comparing the performance parameters, such as apparent power, active and reactive power, THD, and DC voltage balance. The proposed FLC delivered better performance than the PI controller. When using the PI controller, the MMC input voltage is not settled, but when using the FLC, it is in less than 0.4 s. The apparent and active powers are increased when using the FLC. The reactive power compensation is accomplished through the implementation of the FLC. Grid current THD of 4.14% is achieved using FLC which is better than PI's (4.79%). Summarizing, in terms of effectiveness, the proposed design and controller clearly outperform the PI controller.

REFERENCES

[1] S. Liang, Q. Hu, and W. Lee, "A survey of harmonic emissions of a commercial operated wind farm," in *2010 IEEE Industrial and Commercial Power Systems Technical Conference - Conference Record*, Tallahassee, FL, USA, Feb. 2010, https://doi.org/10.1109/ICPS.2010.5489884.

[2] Y. Nagaraja, T. Devaraju, A. M. Sankar, and V. Narasimhulu, "PV and Wind Energy Conversion Exploration based on Grid Integrated Hybrid Generation Using the Cuttlefish Algorithm," *Engineering, Technology & Applied Science Research*, vol. 12, no. 6, pp. 9670–9675, Dec. 2022, https://doi.org/10.48084/etasr.5364.

[3] J. M. Carrasco *et al.*, "Power-Electronic Systems for the Grid Integration of Renewable Energy Sources: A Survey," *IEEE Transactions on Industrial Electronics*, vol. 53, no. 4, pp. 1002–1016, Jun. 2006, https://doi.org/10.1109/TIE.2006.878356.

[4] T. Boghdady, I. A. Sweed, and D. K. Ibrahim, "Performance Enhancement of Doubly-Fed Induction Generator-Based-Wind Energy System," *International Journal of Renewable Energy Research (IJRER)*, vol. 13, no. 1, pp. 311–325, Mar. 2023.

[5] G. D. Marques and M. F. Iacchetti, "DFIG Topologies for DC Networks: A Review on Control and Design Features," *IEEE Transactions on Power Electronics*, vol. 34, no. 2, pp. 1299–1316, Oct. 2019, https://doi.org/10.1109/TPEL.2018.2829546.

[6] J. Hu, Y. He, L. Xu, and B. W. Williams, "Improved Control of DFIG Systems During Network Unbalance Using PI–R Current Regulators,"

IEEE Transactions on Industrial Electronics, vol. 56, no. 2, pp. 439–451, Oct. 2009, https://doi.org/10.1109/TIE.2008.2006952.

[7] J. Hu, H. Nian, B. Hu, Y. He, and Z. Q. Zhu, "Direct Active and Reactive Power Regulation of DFIG Using Sliding-Mode Control Approach," *IEEE Transactions on Energy Conversion*, vol. 25, no. 4, pp. 1028–1039, Sep. 2010, https://doi.org/10.1109/TEC.2010.2048754.

[8] M. K. Bourdoulis and A. T. Alexandridis, "Direct Power Control of DFIG Wind Systems Based on Nonlinear Modeling and Analysis," *IEEE Journal of Emerging and Selected Topics in Power Electronics*, vol. 2, no. 4, pp. 764–775, Sep. 2014, https://doi.org/10.1109/JESTPE.2014.2345092.

[9] V. Narasimhulu, D. V. Ashok Kumar, and Ch. Sai Babu, "Simulation Analysis of Switch Controlled Power Filters for Harmonic Reduction," *International Journal of Applied Engineering Research*, vol. 11, no. 12, pp. 7597–7602, Jun. 2016, https://doi.org/10.37622/IJAER/11.12.2016.7597-7602.

[10] J. Yao, H. Li, Y. Liao, and Z. Chen, "An Improved Control Strategy of Limiting the DC-Link Voltage Fluctuation for a Doubly Fed Induction Wind Generator," *IEEE Transactions on Power Electronics*, vol. 23, no. 3, pp. 1205–1213, Feb. 2008, https://doi.org/10.1109/TPEL.2008.921177.

[11] V. Narasimhulu, D. V. Ashok Kumar, and Ch. Sai Babu, "Recital analysis of multilevel cascade H-bridge based active power filter under load variation," *SN Applied Sciences*, vol. 1, no. 12, Nov. 2019, Art. no. 1621, https://doi.org/10.1007/s42452-019-1669-8.

[12] V. Narasimhulu and K. Jithendra Gowd, "Performance Analysis of Single-Stage PV Connected Three-Phase Grid System Under Steady State and Dynamic Conditions," in *Cybernetics, Cognition and Machine Learning Applications*, Singapore, 2021, pp. 39–46, https://doi.org/10.1007/978-981-33-6691-6_5.

[13] Y. Zhang and T. Jiang, "Robust Predictive Rotor Current Control of a Doubly Fed Induction Generator Under an Unbalanced and Distorted Grid," *IEEE Transactions on Energy Conversion*, vol. 37, no. 1, pp. 433–442, Mar. 2022, https://doi.org/10.1109/TEC.2021.3104410.

[14] V. Narasimhulu, D. V. Ashok Kumar, and Ch. Sai Babu, "Computational intelligence based control of cascaded H-bridge multilevel inverter for shunt active power filter application," *Journal of Ambient Intelligence and Humanized Computing*, Jan. 2020, https://doi.org/10.1007/s12652-019-01660-0.

[15] K. Srilakshmi *et al.*, "Performance Analysis of Artificial Intelligence Controller for PV and Battery Connected UPQC," *International Journal of Renewable Energy Research (IJRER)*, vol. 13, no. 1, pp. 155–170, Mar. 2023.

[16] P. Livinti, "Comparative Study of a Photovoltaic System Connected to a Three-Phase Grid by Using PI or Fuzzy Logic Controllers," *Sustainability*, vol. 13, no. 5, Jan. 2021, Art. no. 2562, https://doi.org/10.3390/su13052562.

[17] G. Todeschini and A. E. Emanuel, "A novel control system for harmonic compensation by using Wind Energy Conversion based on DFIG technology," in *2010 Twenty-Fifth Annual IEEE Applied Power Electronics Conference and Exposition (APEC)*, Palm Springs, CA, USA, Oct. 2010, pp. 2096–2103, https://doi.org/10.1109/APEC.2010.5433525.

[18] L. Benaaouinate, M. Khafallah, D. Voyer, A. Mesbahi, and T. Bouragba, "Nonlinear Control Based on Fuzzy Logic for a Wind Energy Conversion System Connected to the Grid," *International Journal of Renewable Energy Research*, vol. 10, no. 1, pp. 193–204, Mar. 2020.

[19] V. Narasimhulu, D. V. Ashok Kumar, and Ch. Sai Babu, "Fuzzy Logic Control of SLMMC-Based SAPF Under Nonlinear Loads," *International Journal of Fuzzy Systems*, vol. 22, no. 2, pp. 428–437, Mar. 2020, https://doi.org/10.1007/s40815-019-00622-0.

[20] C. Liu, D. Xu, N. Zhu, F. Blaabjerg, and M. Chen, "DC-Voltage Fluctuation Elimination Through a DC-Capacitor Current Control for DFIG Converters Under Unbalanced Grid Voltage Conditions," *IEEE Transactions on Power Electronics*, vol. 28, no. 7, pp. 3206–3218, Jul. 2013, https://doi.org/10.1109/TPEL.2012.2223829.

[21] O. Georges *et al.*, "Assessment of the Conventional Energy Potential in Cameroon: The use of Wind, Small Hydro and Solar Technologies as Alternatives Solutions," *International Journal of Renewable Energy Research (IJRER)*, vol. 13, no. 1, pp. 77–86, Mar. 2023, https://doi.org/10.20508/ijrer.v13i1.13339.g8663.

[22] J. Rodriguez, J.-S. Lai, and F. Z. Peng, "Multilevel inverters: a survey of topologies, controls, and applications," *IEEE Transactions on Industrial Electronics*, vol. 49, no. 4, pp. 724–738, Dec. 2002, https://doi.org/10.1109/TIE.2002.801052.

[23] V. Narasimhulu, D. V. Ashok Kumar, and Ch. Sai Babu, "State of Art Review of Various Control Methods for Cascade H-Bridge 5-Level Inverter to Mitigate Harmonics," *International Journal of Control Theory and Applications*, vol. 10, no. 28, pp. 1–7, May 2017.

[24] V. Narasimhulu, D. V. Ashok Kumar, and Ch. Sai Babu, "Comparative Simulation Analysis of Harmonics in Line-Line Output Voltage of Multilevel Inverters for Different Modulation Indices," *International Journal of Control Theory and Applications*, vol. 10, no. 5, pp. 289–296, Jan. 2017.

[25] Y. Zou, M. E. Elbuluk, and Y. Sozer, "Simulation Comparisons and Implementation of Induction Generator Wind Power Systems," *IEEE Transactions on Industry Applications*, vol. 49, no. 3, pp. 1119–1128, Feb. 2013, https://doi.org/10.1109/TIA.2013.2253531.

[26] S. Puchalapalli and B. Singh, "A Novel Control Scheme for Wind Turbine Driven DFIG Interfaced to Utility Grid," *IEEE Transactions on Industry Applications*, vol. 56, no. 3, pp. 2925–2937, Feb. 2020, https://doi.org/10.1109/TIA.2020.2969400.

[27] V. Narasimhulu, D. V. Ashok Kumar, and Ch. Sai Babu, "Recital Analysis of Modular Multilevel Converter Based Shunt Active Power Filter," *Journal of Mechanics of Continua and Mathematical Sciences*, no. Special 5, pp. 181–192, Jan. 2020, https://doi.org/10.26782/jmcms.spl.5/2020.01.00016.

[28] M. A. Perez, S. Bernet, J. Rodriguez, S. Kouro, and R. Lizana, "Circuit Topologies, Modeling, Control Schemes, and Applications of Modular Multilevel Converters," *IEEE Transactions on Power Electronics*, vol. 30, no. 1, pp. 4–17, Jan. 2015, https://doi.org/10.1109/TPEL.2014.2310127.

[29] T. Demirdelen, R. I. Kayaalp, and M. Tumay, "A Modular Cascaded Multilevel Inverter Based Shunt Hybrid Active Power Filter for Selective Harmonic and Reactive Power Compensation Under Distorted/Unbalanced Grid Voltage Conditions," *Engineering, Technology & Applied Science Research*, vol. 6, no. 5, pp. 1133–1138, Oct. 2016, https://doi.org/10.48084/etasr.777.

[30] S. L. S. Louarem, D. E. C. Belkhiat, T. Bouktir, and S. Belkhiat, "An Efficient Active and Reactive Power Control of DFIG for a Wind Power Generator," *Engineering, Technology & Applied Science Research*, vol. 9, no. 5, pp. 4775–4782, Oct. 2019, https://doi.org/10.48084/etasr.3007.